Optimization of Biased PT-Symmetric Plasmonic Directional Couplers

José R. Salgueiro and Yuri S. Kivshar

(Invited Paper)

***Abstract*—We study a plasmonic directional coupler with a metallic cladding and dielectric core in the presence of balanced gain and loss, and demonstrate that such a photonic structure can possess the parity-time (PT) symmetry even when optical losses in metal are taken into account. We analyze the modal dispersion of the coupler when losses in metal are negligible and then study how substantially increased losses modify the modal dispersion and coupler's properties. For realistic parameters, we demonstrate a novel approach for recovering the property of the PT-symmetry by introducing unbalanced loss and gain in both cores of the coupler.**

***Index Terms*—Parity-time symmetry, plasmonics, optical couplers, losses, complex modes.**

I. Introduction

RECENTLY, we observe a substantial progress in developing miniaturized integrated optical components to improve energy efficiency and achieve direct interfacing with electronic circuits. The incorporation of optical interconnects on memory and processing computer modules is recognized by leading manufacturers, including IBM, as a path towards lower power consumption and increased performance. Furthermore, plasmonic circuits, based on hybrid metal-dielectric structures, can facilitate such integration by providing strong confinement of light for efficient interfacing with nanoscale electronic interconnects. However, metals unavoidably introduce absorption at optical wavelengths. This problem calls for the implementation of active plasmonic circuits, where gain can provide signal amplification while loss can be also useful for suppression of undesirable interference. Although significant progress has been achieved through the incorporation of active gain media, it remains a challenging problem of key importance to develop photonic-plasmonic circuits with ultrafast tunability of gain, operating across a broad range of optical frequencies for compatibility with different interconnects.

One of the potential solutions of this problem is based on the so-called parity-time (PT) symmetric systems, recently introduced in photonics, where novel possibilities are offered for controlling a flow of light in integrated photonic devices. Similar to quantum mechanics, the PT symmetric photonic systems are characterized by complex potentials with a symmetric real part and antisymmetric imaginary part of the optical dielectric constant (or the refractive index playing a role of an effective potential in quantum mechanics) [1]–[5]. The key property of such a PT-symmetric photonic system is the fact that even though the permittivity is a complex number, the propagation constant is real, i.e. the eigenvalue spectrum is described by real numbers. The frequency of light propagating in a medium with balanced gain and loss determines whether a particular mode is real or complex, existing what are known as *exceptional points* (EP) where the propagation constant changes from real to complex (where the PT-symmetry is defined as being broken) and vice versa, also changing at these points the propagation characteristics of the mode.

A simple practical realization of a PT-symmetric photonic system is a directional optical coupler formed by two geometrically identical parallel waveguides with the same value of the refractive index but accumulating loss and gain in an exactly opposite amount [6]. Overpassing an EP would break the PT symmetry. For example, changing the frequency of the optical source used to excite one of the waveguides can transform the symmetric coupling between the waveguides into an asymmetric coupling [7] where light remains trapped mainly in one of the waveguides or demonstrate nonreciprocal behavior.

The actuation on the geometrical parameters (device design) as well as a change of loss and gain (real-time control) allow placing one particular mode in the real or complex part of the spectrum, i.e. moving the EPs along the frequency axis making such systems versatile and reconfigurable. Additionally, this functionality can be enhanced by introducing nonlinear effects, i.e. choosing appropriate materials and using high power sources. In such a way, the PT symmetric systems can be employed to realize interesting applications such as optical switching [8]–[10], demultiplexing of signals [11], or integrated lasers [12]–[15].

Another interesting proposal is to combine the PT-symmetry properties with plasmonics. The development of systems containing metals has opened photonics to the world of nanoscale systems since they demonstrate possibility to confine optical fields to orders of magnitude below the wavelength [16]–[18]. The reason is the coupling of optical waves with the plasma oscillations of metals whose simplest practical realizations are *surface plasmon polaritons* created by an optical mode propagating along an interface between dielectric and metal media.

Manuscript received January 20, 2016; revised April 12, 2016; accepted April 12, 2016. This work was supported in part by the Xunta de Galicia (Spain) under the project no. GPC2015/019 and in part by the Australian Research Council.

J. R. Salgueiro is with the Departamento de Física Aplicada, Universidade de Vigo, 32004 Ourense, Spain (e-mail: jrs@uvigo.es).

Y. S. Kivshar is with Nonlinear Physics Center, Research School of Physics and Engineering, The Australian National University, Canberra, ACT 2601, Australia (e-mail: ysk@internode.on.net).

Color versions of one or more of the figures in this paper are available online at http://ieeexplore.ieee.org.

Digital Object Identifier 10.1109/JSTQE.2016.2555283

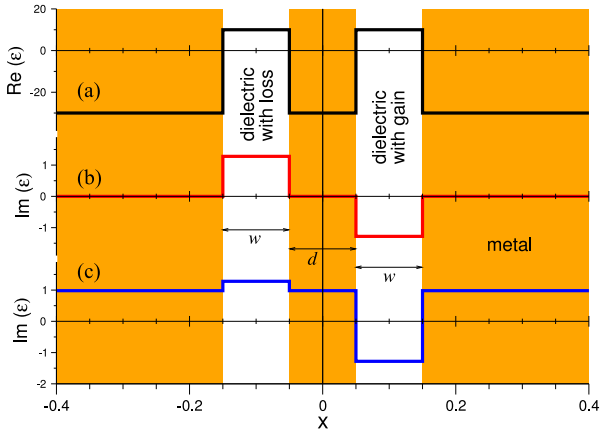

Fig. 1. A sketch of a directional coupler with metallic cladding (shaded) and dielectric cores. Overprinted are the dielectric functions: (a) real part, (b) imaginary part for vanishing cladding losses, and (c) imaginary part for realistic cladding losses.

Hybrid plasmonic and PT-symmetric systems have been already studied by several groups [19]–[21] as well as their propagation properties and potential applications for integrated optics and optoelectronics. In order to combine plasmonics with the PT-symmetry functionality, we may consider a typical structure of a plasmonic directional coupler where two dielectric cores with loss and gain are bounded by metallic claddings (see Fig. 1), which was in fact studied earlier [20] for negligible losses in the metallic claddings.

A very important feature of plasmonic systems is a high level of losses they demonstrate. This leads not only to optical power loss via electronic collisions but also to a complete modification of the modal spectrum of waveguides which should be treated by using the complex modes [22]–[24]. Also, other undesired effects arise as for instance a decrease of the power switching efficiency in nonlinear couplers [25]. Regarding the PT-symmetric plasmonic coupler, it may be expected that the study could be in principle similar, considering or neglecting losses, however this is not the case. In fact, losses in metallic claddings break the PT-symmetry as now the imaginary part of the dielectric function is no longer an antisymmetric function [see Fig. 1, function (c)]. In fact, it is biased by the introduction of a nonzero imaginary dielectric constant at the metallic claddings. This induces the suppression of EPs so that all the modes become complex, and consequently most of the functionalities based on the PT-symmetry no longer remain. In this paper, we explore the possibility of compensating, at least partially, this undesired effect, by means of a proper balance between loss and gain introduced in the dielectric cores. Our aim is to recover the original effects of the PT-symmetry, at least in particular regions of the spectrum, to achieve the original functionalities of the photonic system.

In what follows, we describe our system, the basic modeling equations and the way to obtain the complex modes (Section II). We also describe the dispersion diagram of the lowest-order coupler modes when losses are negligible (Section III). Then, in Section IV, we reveal how the dispersion diagram changes when losses are made substantially larger. In Section V we study the effect of introducing a detuning on gain and loss in both the cores to recover the PT-symmetry properties in the plasmonic system. Finally, in Section VI some simulations are presented to illustrate and demonstrate the behavior of the PT-symmetric system, the effects of metal losses and the performance of the technique use to compensate them.

II. Numerical Modeling

We consider a directional coupler with two dielectric cores of the same width w, separated a distance d, and metallic claddings whose planar structure lies in the x-direction as the one shown in Fig. 1, and is described by the complex dielectric function $\epsilon(x)$. We start with Maxwell's equations and search for modal-type solutions for the electric and magnetic fields $\tilde{\mathbf{E}}(\mathbf{r},t)$ and $\tilde{\mathbf{H}}(\mathbf{r},t)$ of frequency ω and propagating along the direction of the z-axis,

$$\tilde{\mathbf{E}}(\mathbf{r},t) = \mathbf{E}(x)\exp\left[i(\beta z-\omega t)\right], \tag{1}$$

$$\tilde{\mathbf{H}}(\mathbf{r},t) = \mathbf{H}(x)\exp\left[i(\beta z-\omega t)\right]/(\mu_0 c), \tag{2}$$

being β the propagation constant, μ_0 the magnetic permeability and c the speed of light in vacuum. On the other hand t stands for time and the spatial variables $\mathbf{r}=(x,y,z)$ are adimensional after being rescaled by the vacuum wavenumber $k_0=\omega/c$. We focus on the TM mode and so we take fields with specific components $\mathbf{E}=E_x\hat{\mathbf{x}}+i\,E_z\hat{\mathbf{z}}$, $\mathbf{H}=H_y\hat{\mathbf{y}}$. In this way, after replacing the expressions (1) and (2) into the Maxwell's equations we come to the following set of ordinary differential equations

$$\partial_x H_y = \epsilon E_z, \tag{3}$$

$$\partial_x E_z = -(1-\beta^2/\epsilon)H_y, \tag{4}$$

as well as to the relationship $\beta H_y=\epsilon E_x$.

The system is modeled piecewise through the dielectric function. For the metallic claddings we use the simple dispersive model from Drude

$$\epsilon_m(\omega)=\epsilon_\infty-\frac{\omega_p^2}{\omega^2+i\Gamma\omega}, \tag{5}$$

where ω_p and Γ describe respectively the plasma frequency of collective electronic oscillations and the electronic collision frequency responsible for losses. Parameter ϵ_∞ stands for the high frequency limit of ϵ which can be taken as $\epsilon_\infty=1$ at low and moderate frequencies. For usual metals at optical frequencies the value of $\epsilon_m(\omega)=\epsilon_m'(\omega)+i\epsilon_m''(\omega)$ presents a negative and fairly large real part and a relatively small imaginary part. On the other hand both dielectric cores (that we label 1 and 2) are modeled by a complex dielectric constant $\epsilon_{1,2}=\epsilon'+i\epsilon_{1,2}''$. We assume that core 1 presents optical loss (so that $\epsilon_1''>0$) and core 2 optical gain (so $\epsilon_2''<0$).

Since the dielectric function is complex both electric and magnetic fields are in general also complex, $E_z(x)=e'(x)+ie''(x)$, $H_y(x)=h'(x)+ih''(x)$, and the same is valid for the propagation constant $\beta=\beta'+i\beta''$. As the system is linear there exist an analytical solution for the modal fields which can be obtained at every layer of the structure and takes the form [26], [27]

$$H_y(x)=C_{n,1}\exp(\mu_n x)+C_{n,2}\exp(-\mu_n x), \tag{6}$$

being the other component E_z described by a similar expression. In the equation above n labels the different layers being $\mu_{1,3,5} = (\beta^2 - \epsilon_m)^{1/2}$ for metallic claddings and $\mu_{2,4} = (\beta^2 - \epsilon)^{1/2}$ for dielectric cores. $C_{n,1}$ and $C_{n,2}$ are constants to be fixed by applying the boundary conditions. Such conditions require a decreasing exponential behavior for $x \to \pm\infty$ and the continuity of both H_y and E_z at the interfaces between layers.

Although the solution is analytical its calculation is not exempt of certain difficulty. The application of the different boundary conditions leads to a transcendent algebraic equation for the eigenvalue β which has to be numerically solved in the complex plane. Though there are methods suitable for this purpose [27], [28], we decided to solve the system described by Eqs. (3) and (4) numerically by means of a relaxation algorithm exploiting a code previously made for nonlinear plasmonic waveguides [24], [29]. In such a way, Eqs. (1) and (2) are discretized in finite differences in both cores and solved using the boundary conditions related to the continuity of fields between cores and claddings

$$\left(\beta^2 - \epsilon_m\right)^{1/2} H_y \pm \epsilon_m E_z = 0, \tag{7}$$

where the plus is to be used for the cladding-core boundaries and the minus sign at core-cladding boundaries. In contrast to a nonlinear system which has a solution for any value of the propagation constant β, the linear system has solutions only for particular values of β (eigenvalues). To find such values [30] we consider β as another function (constant) to be sought together with the field components H_y and E_z using the equations (1) and (2) and the boundary conditions (7). That means an additional equation is needed $\partial_x \beta = 0$ (condition for a constant function) together with an additional boundary condition. This condition reduces to fix any of the field components to an arbitrarily value at any point of the domain (typically one of the boundaries). This is due to the fact that a scaling of the fields by a constant does produce another solution of the system because it is linear. Once the solutions are obtained at the cores, they are augmented to the cladding using the analytical expression (6).

III. Modal Dispersion

First we start with the case of negligible losses in metallic claddings, already studied by Alaeian *et al.* [20]. In such a case if we take balanced loss and gain in the cores $\epsilon_2'' = -\epsilon_1''$ we have a perfect PT-symmetric system. For the system parameters we chose core width $w = 0.1$ and inter-core distance $d = 0.1$ (both in normalized units). For the core dielectric constant we took $\epsilon' = 10.2$ and $\epsilon_1'' = 1.28$, following the mentioned reference [20], to obtain comparable results. In order to give a reference in real units, the values above correspond to $(\tilde{d}, \tilde{w}) = (d, w)\lambda/2\pi = 13$ nm when a wavelength of $\lambda = 800$ nm is chosen, and $\tilde{d} = \tilde{w} = 25$ nm for $\lambda = 1.55\,\mu$m, the standard wavelength of the third telecommunications window. This confirms those dimensions as realistic, and the fact that the thickness of the inter-core layer is below the limit of ~ 100 nm which represents a natural limit for the device to work.

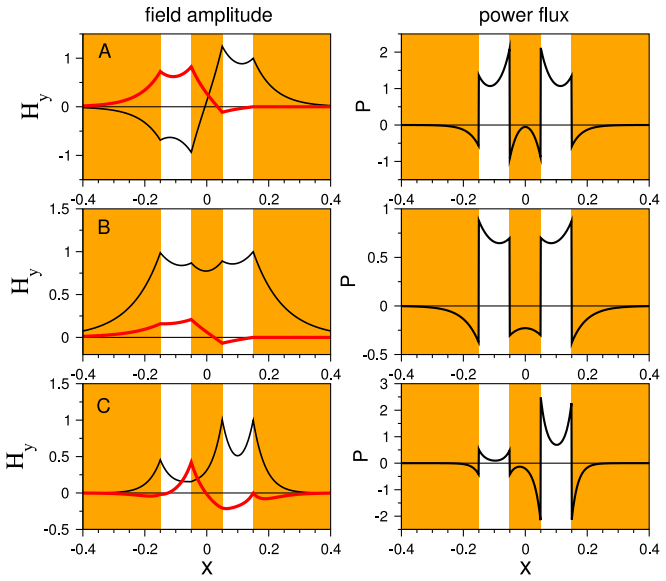

Fig. 2. Some examples of the complex modes. On the left column the real (thin black line) and imaginary (thick red line) parts of the magnetic component is plotted for three different modes. On the right column it is plotted the power flux for the same respective modes. Labeling letters correspond to the points in Figs. 3(a) and 4(a).

It is important to notice that the value of optical gain $\epsilon'' = -1.28$ is large in practice, according to the usual gain values achievable today with standard semiconductor technologies. In fact, typical values for gain [12], [19] are in the range of few hundreds of cm^{-1}, giving values of ϵ'' about an order of magnitude smaller for a wavelength in the visible region. We chose the value above, however, to make our results comparable with the non lossy case studied in Ref. [20], assuming that the results are qualitatively significant and the essence of the compensation strategy developed in Section V does not change. If the necessary values of gain are not achievable in practice (what will also depend on the loss value on metallic claddings) the compensation can be achieved at least partially and this will suppose an advance anyway.

The plasma frequency is chosen as $\omega_p = 1$ so the frequency in expression (5) can be understood as a relative frequency ω/ω_p. To give a reference value let us consider silver (a commonly used metal in plasmonics). From Ref. [31] we find $\epsilon' = -29.7$ and $\epsilon'' = 0.981$ for a wavelength $\lambda = 800$ nm. From these values we obtain $\omega_p = 1.31 \times 10^{16}$ Hz and $\Gamma = 7.53 \times 10^{13}$ Hz for the plasma and electronic collision frequencies. This indicates that a realistic value for Γ could be about two magnitude orders below the plasma frequency. Similar results can also be obtained from Ref. [32]. Also in both references values for other wavelengths as well as for other metals commonly used in plasmonics, like gold or aluminum, can be found.

In Fig. 2 (left column) we show examples of three of the real modes of the system. Modes labeled A and B are the typical lowest order modes for a coupler, the antisymmetric (A) which for plasmonic couplers is also the fundamental [33] and the symmetric (B), both calculated for $\omega = 0.2\,\omega_p$. In the right column it is plotted the power flux in the z-direction, given by

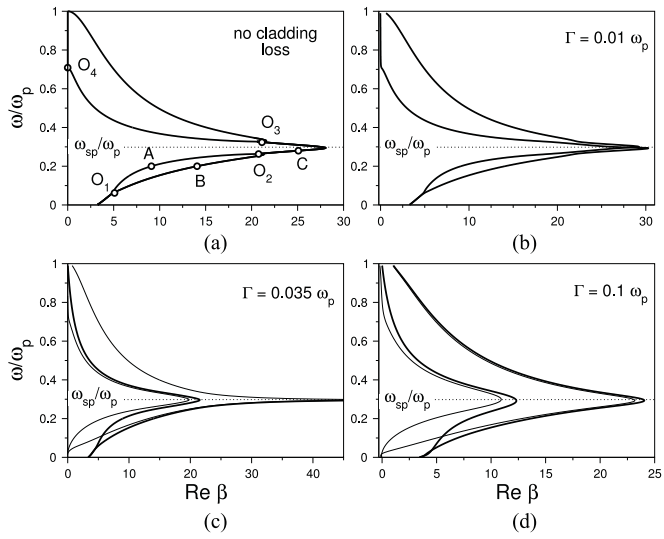

Fig. 3. Dispersion diagrams showing frequency versus the real part of the propagation constant for negligible cladding losses (a) and for three different cases of low, moderate and high loss (b)–(d). Labels A, B, C on subfigure (a) correspond to modes showed in Fig. 2. O_1–O_4 are exceptional points.

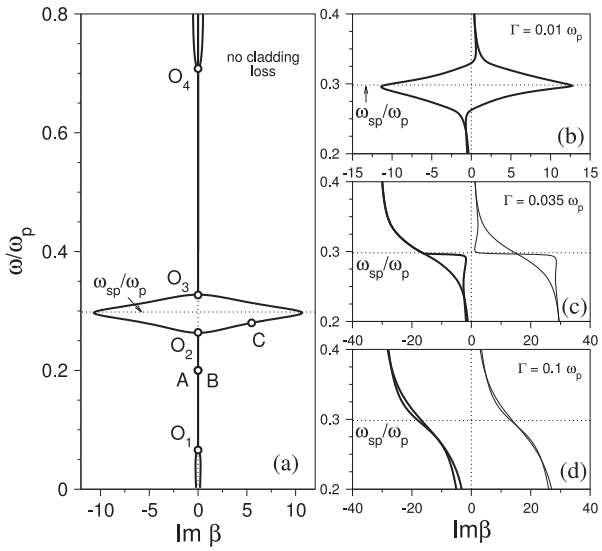

Fig. 4. Dispersion diagrams where frequency is plotted versus imaginary part of propagation constant for the non lossy case (a) and for the three different cases correspondent to low, moderate and large loss (b)–(d). Labels A, B, C on subfigure (a) correspond to modes showed in Fig. 2. O_1–O_4 are exceptional points.

the expression

$$P(x) = (\mathbf{E} \times \mathbf{H}^*)\,\hat{\mathbf{z}} = \beta\left(|H_y(x)|^2/\epsilon\right). \tag{8}$$

Note that these modes present complex field components but the propagation constant is real as shown in Figs. 3(a) and 4(a) where the dispersion diagrams of the modes are plotted respectively against real and imaginary part of the propagation constant. This means the total power flux $P = \int P(x)\,dx$ remains constant upon propagation and the coupler behaves symmetrically as follows from the symmetry of the power flux function, so that power periodically transfers from one waveguide to the other.

At low enough frequencies or for higher frequencies closer to the surface plasmon resonance ω_{sp} both modes merge in an EP [points O_1 and O_2 in Figs. 3(a) and 4(a)] where PT-symmetry is broken and asymmetric complex modes (complex propagation constant) are originated. An example is in Fig. 2(C). Now power flux is asymmetric indicating that a larger amount of power will remain in the gain core as it propagates.

Higher order modes are also real for frequencies above the surface plasmon resonance from EP O_3 up to EP O_4 as shown in Figs. 3(a) and 4(a).

IV. Losses in Metallic Cladding

When losses in metallic claddings are present the system is no longer PT-symmetric and the EPs disappear from the dispersion diagram. In Figs. 3(b)–(d) and 4(b)–(d) such diagrams are shown for three different loss levels, from small to large, described in terms of the electronic collision frequency parameter. These values were chosen taking into account the reference parameters calculated in the previous section for silver at $\lambda \approx 800$ nm. In fact at such wavelength $\Gamma = 0.0057\,\omega_p$. This means that a value of $\Gamma \sim 0.01\,\omega_p$ is realistic, although this value may change quite for different wavelengths and/or metals.

For small loss the curves just only deform slightly respect to those corresponding to the non lossy case. With increasing losses the shape of the curves dramatically changes [22]–[24], all the modes are now complex and no longer come in complex conjugate pairs. The original degeneracy is broken and different modes merge together at $\omega = \omega_{sp}$ and become indistinguishable. Generally, every mode joins to the next order mode presenting the same symmetry.

V. Compensating the Losses

The possibility of actuating on the loss and gain levels of both cores brings the chance of changing the behavior of the system. In principle operating on these parameters does not make possible to get a full PT-symmetric system. However the effect of reducing loss in the first core or increasing gain in the second intuitively reduces the effect of cladding loss as it pushes the imaginary part of the dielectric function in the opposite direction producing a balancing effect.

In order to carry out a study on these effects we performed a set of simulations on the system presenting collision frequency $\Gamma = 0.01$ to check whether the dispersion diagrams reshape so that the imaginary part of the propagation constant can be reduced to values close to zero. For this we increased gain in the second core at small steps maintaining the value of loss for the first one and recalculating the dispersion diagram in each case. A similar study was then performed maintaining gain in the second core and decreasing loss at small steps in the first one. A third study was done increasing gain and decreasing loss at a time. To evaluate the grade of recovering of the real propagation constant we define a *complexity parameter*, η, as the averaged value of the imaginary part of the propagation constant for a frequency interval where it was originally zero before losses at

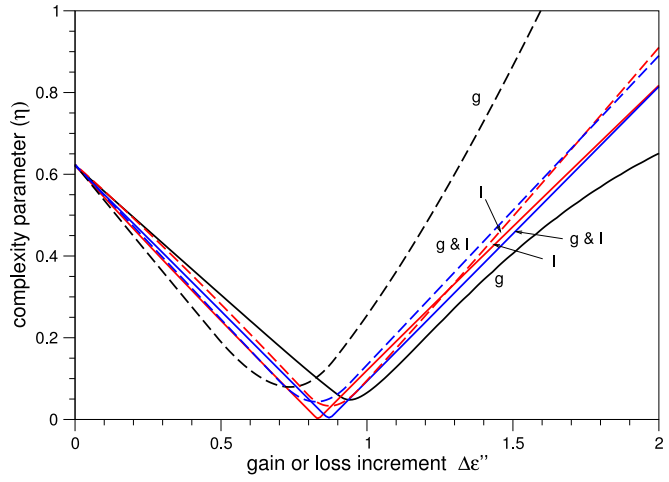

Fig. 5. Complexity parameter for different values of the gain/loss asymmetry. Line labels indicate the cases of increasing gain at the second core (label *"g"*, black line), decreasing loss at the first core (label *"l"*, red line) and the combination of both actions (label *"g & l"*, blue lines), but introducing half the effect at each of the cores. Continuous lines are for the symmetric mode and dashed lines for the antisymmetric mode.

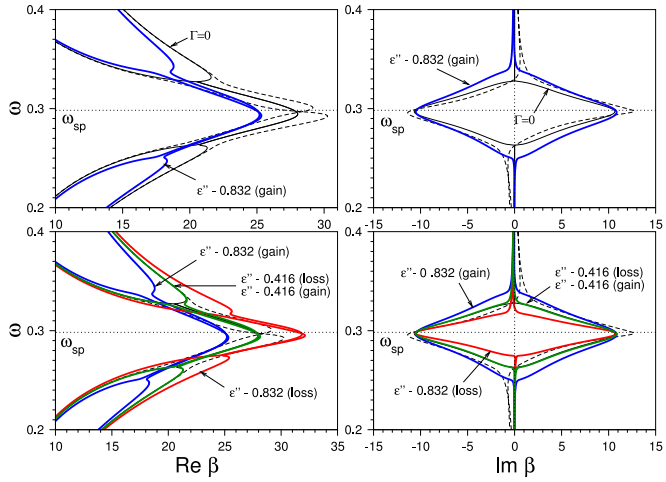

Fig. 6. Top row plots the dispersion diagram (frequency versus respectively the real and imaginary parts of the propagation constant) for the unbalanced gain/loss system correspondent to an increase of gain optimized for obtaining modes with a minimum imaginary part at frequencies below the surface plasmon frequency [thick (blue) lines]. Also the dispersion curves of modes of the balanced system are plotted for comparison, for the negligible cladding losses (continuous thin line) and for realistic cladding losses (dashed line). Bottom row plots the dispersion curves for the optimized unbalanced system for three different cases of optimization: for an increase of gain, a decrease of loss and for a combination of both actions.

claddings were taken into account

$$\eta = \frac{1}{\omega_2 - \omega_1} \int_{\omega_1}^{\omega_2} |\mathrm{Im}\,\beta|\, d\omega. \tag{9}$$

According to the dispersion diagrams of Fig. 4(a) and (b), we reasonably chose $\omega_1 = 0.2\,\omega_p$ and $\omega_2 = 0.25\,\omega_p$ to evaluate the parameter for the lowest order modes, expecting a value close to zero when the system behaves as PT-symmetric. In Fig. 5 the value of η is plotted versus the gain or loss increment for the three different cases: gain increase at the core showing gain, $\epsilon'' - \Delta\epsilon''$ (beware ϵ'' is negative to implement gain), loss decrease at the core showing loss, $\epsilon'' - \Delta\epsilon''$ (in this case ϵ'' is positive) and a combination of both effects increasing gain and decreasing loss at the respective cores an amount $\Delta\epsilon''/2$ each. We see the curves go through a minimum which is the optimal value at which the PT-symmetric behavior is best recovered. As closest to zero is the minimum the better the PT-symmetric behavior is recovered. Generally it is possible to get a very low minimum when losses at claddings are weak (parameter Γ is small). For increasing metal losses the value at the minimum also increases. Interestingly the symmetric mode recovers the PT-symmetry better than the antisymmetric one as the minima for the symmetric mode reach lower values (continuous lines) than for the antisymmetric (dashed lines).

From Fig. 5 we appreciate the minimum is for a value of the gain increment around $\Delta\epsilon'' = 0.8$ (it is different for the symmetric and antisymmetric modes, but the mean value is close to 0.8). For such a gain increment a nearly zero β_2 is recovered for frequencies in the interval $[0.2\,\omega_p, 0.25\,\omega_p]$. This is shown in the top row of Fig. 6 where the dispersion diagrams are presented (thick lines) overprinted to the original ones (dashed lines) and those for a lossless metal (thin lines). It is seen that the EP below ω_{sp} is practically recovered. The same can be achieved for the EP over ω_{sp} but for a different value of the gain increment.

On the other hand this compensation effect can be also obtained decreasing loss in the first core or simultaneously decreasing loss in the first core and increasing gain in the second one as shown in Fig. 5. In the last case, the variation necessary for every core is half the one needed when operating on a single core. Bottom row of Fig. 6 shows a comparison between the results obtained from these three different strategies. In every case, the EP is recovered and the unique difference is the position (frequency) where it lays. This means that it is still possible to place the EP actuating on the levels of loss and gain, as was in full PT-symmetric systems.

VI. Light Propagation and Switching

We have carried out some numerical simulations using the finite-difference time-domain technique to check the PT-symmetry behavior of the system, the effect of losses in the metallic claddings and the loss compensation effect of the unbalanced gain/loss set in both cores. For this, we have made a specific code to deal with complex fields and used specific models to describe the permittivity of the medium at cores and claddings respectively. Both modelings are introduced into the Ampère's law $\epsilon\partial_t \mathbf{E} = \nabla \times \mathbf{H} - \mathbf{J}$ equation as a term of current.

The metallic claddings were modeled using the Drude model [Eq. (5)] which is implemented as an additional differential equation for a displacement current ($\mathbf{J} = \partial_t \mathbf{P}$), $\partial_t \mathbf{J} + \Gamma \mathbf{J} = \omega_p \mathbf{E}$ which is solved together with the Maxwell's equations using Young's direct algorithm [34].

On the other hand the cores are modeled by a simple homogeneous medium of constant real permittivity, introducing loss and gain through a conductivity parameter σ which is added to the Maxwell's equations as a current term of the form $\mathbf{J} = \sigma \mathbf{E}$.

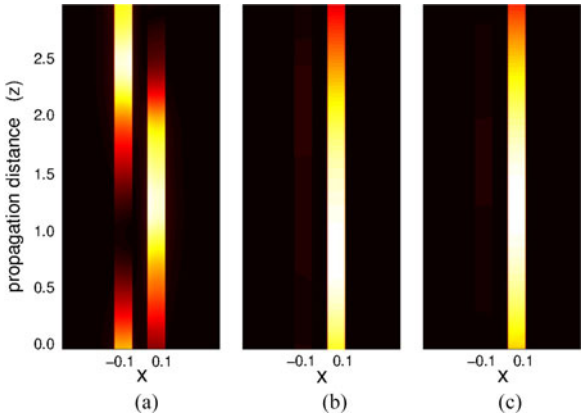

Fig. 7. Time-averaged Poynting vector in the z-direction for the plasmonic PT-symmetric coupler with no loss in the metallic cladding. Left core presents loss while right core presents an equivalent gain. (a) Case for $\omega = 0.086\,\omega_p$, (b) case for $\omega = 0.14\,\omega_p$ (left core excited) and (c) case for $\omega = 0.14\,\omega_p$ (right core excited). Brighter colors represent higher power. Maximum power density (correspondent to white color) reaches values of 1.3 (a), 70 (b) and 1300 (c) in relative units (maximum input power density at $z = 0$ is the unity).

The σ parameter is related to the imaginary part of the permittivity as $\epsilon'' = \sigma/\omega$. In order to chose a constant value for the conductivity parameter, which should be valid for the whole frequency range of interest (up to $\omega_{sp} \approx 0.3\,\omega_p$), we evaluate it for an intermediate frequency $\omega = 0.2\,\omega_p$. So taking the value of $\epsilon'' = \pm 1.28$ used for the eigenvalue calculation above, we obtain $\sigma = \pm 1.28 \times 0.2 = \pm 0.256$. The sign of the conductivity parameter determines whether the core behaves lossy (plus sign) or shows gain (minus sign).

As the simulation progresses the z-component of the Poynting vector [Eq. (8)] is computed at every point of the domain and averaged over the necessary number of time steps to accumulate a time equal to three wave periods $T = 3 \times 2\pi/\omega$.

The first set of simulations are performed neglecting losses at the claddings and they are intended to check the behavior of the system when the EP is overpassed. In Fig. 7 we show three different simulations when one of the cores is excited by a Gaussian beam of amplitude unity and width $w_s = 0.05$ (half of core width). For the first simulation [Fig. 7(a)] the system presents PT-symmetry (quasi-real propagation constant) and so power flux experiments the typical beating between both cores of the coupler. When frequency is increased, however, the system overpasses the EP, beating is suppressed and power remains on the gain-core, independently of which of the cores is initially excited, lossy one [Fig. 7(b)] or gain one [Fig. 7(c)]. This power on the gain-core will grow exponentially in time as an effect of the net supply of energy to the system.

It is important to note that the system modeling in both time and frequency domains are not equivalent. In fact, in frequency domain we modeled the system by a piecewise constant complex permittivity, calculating every mode for a fixed frequency. In time domain simulations, however, the strong dispersion of metals was taken into account. Additionally the dielectric cores are modeled by a fixed effective conductivity parameter. According to this, both studies lead to differences, for instance in the position of the EPs.

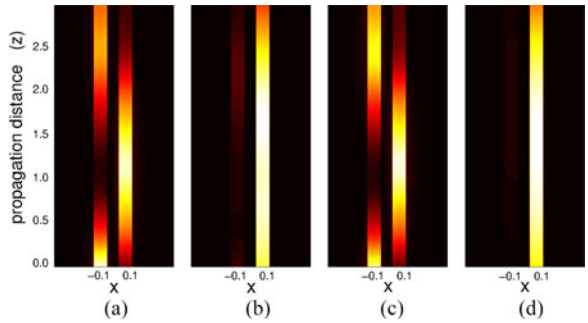

Fig. 8. Time-averaged z-component of the Poynting vector considering a lossy metal at the claddings. (a), (b) Simulations for $\omega = 0.052\,\omega_p$ and $\omega = 0.12\,\omega_p$ respectively for both regimes of unbroken and broken symmetry respectively. (c), (d) Same but for $\omega = 0.052\,\omega_p$ and $\omega = 0.086\,\omega_p$ and with gain in right core increased to balance the effect of cladding loss. Brighter colors represent higher power. Maximum power density correspondent to white color reaches values of 1 (a), 11 (b), 1 (c) and 210 (d) in relative units. (maximum input power density at $z = 0$ is the unity).

When losses in claddings are present a new scenario arises. Losses produce a progressive decreasing of the field amplitude which leads to its decay after a certain propagation distance. Apart from this, if losses are not too high, the system may behave as PT-symmetric and the beating of light between both cores is observed [Fig. 8(a)]. Again, further away from the EP coupling is suppressed, and power remains on the gain-core [Fig. 8(b)]. The effect of compensation of losses improves the undesired decrease of field amplitude due to the loss in the metal, avoiding it from decaying in a short distance as is depicted in Fig. 8(c) and (d) where the simulation is shown when gain at the right core is increased by $\Delta\epsilon'' = 0.832$. On the other hand the transition between unbroken and broken symmetry takes place at a different frequency, particularly at a lower frequency for the simulation shown.

VII. Conclusion

Here, we have made a step towards the practical application of plasmonic directional couplers with metallic claddings and dielectric cores in the presence of balanced gain and loss. We have demonstrated that even when optical losses in metal are taken into account, the coupler can operate in the regime of PT-symmetry recovering some properties of conservative systems. We have analyzed the modal dispersion with and without the losses in metal and described the effect of losses on the optical modes and their properties. For realistic parameters, we have demonstrated a novel approach for recovering the PT-symmetric behavior by introducing an unbalanced loss and gain in both coupler cores.

References

[1] S. Klaiman, U. Günther, and N. Moiseyev, "Visualization of branch points in $\mathcal{PT}$-symmetric waveguides," *Phys. Rev. Lett.*, vol. 101, Aug. 2008, Art. no. 080402. [Online]. Available: http://link.aps.org/doi/10.1103/PhysRevLett.101.080402

[2] K. G. Makris, R. El-Ganainy, D. N. Christodoulides, and Z. H. Musslimani, "Beam dynamics in $\mathcal{PT}$ symmetric optical lattices," *Phys. Rev. Lett.*, vol. 100, Mar. 2008, Art. no. 103904. [Online]. Available: http://link.aps.org/doi/10.1103/PhysRevLett.100.103904

[3] A. Guo *et al.*, "Observation of $\mathcal{PT}$-symmetry breaking in complex optical potentials," *Phys. Rev. Lett.*, vol. 103, Aug. 2009, Art. no. 093902. [Online]. Available: http://link.aps.org/doi/10.1103/PhysRevLett.103.093902
[4] S. Longhi, "Bloch oscillations in complex crystals with $\mathcal{PT}$ symmetry," *Phys. Rev. Lett.*, vol. 103, Sep. 2009, Art. no. 123601. [Online]. Available: http://link.aps.org/doi/10.1103/PhysRevLett.103.123601
[5] X. Luo *et al.*, "Pseudo-parity-time symmetry in optical systems," *Phys. Rev. Lett.*, vol. 110, Jun. 2013, Art. no. 243902. [Online]. Available: http://link.aps.org/doi/10.1103/PhysRevLett.110.243902
[6] R. El-Ganainy, K. G. Makris, D. N. Christodoulides, and Z. H. Musslimani, "Theory of coupled optical PT-symmetric structures," *Opt. Lett.*, vol. 32, no. 17, pp. 2632–2634, Sep. 2007. [Online]. Available: http://ol.osa.org/abstract.cfm?URI=ol-32-17-2632
[7] A. Lupu, H. Benisty, and A. Degiron, "Switching using pt symmetry in plasmonic systems: Positive role of the losses," *Opt. Express*, vol. 21, no. 18, pp. 21651–21668, Sep. 2013. [Online]. Available: http://www.opticsexpress.org/abstract.cfm?URI=oe-21-18-21651
[8] Z. H. Musslimani, K. G. Makris, R. El-Ganainy, and D. N. Christodoulides, "Optical solitons in $\mathcal{PT}$ periodic potentials," *Phys. Rev. Lett.*, vol. 100, Jan. 2008, Art. no. 030402. [Online]. Available: http://link.aps.org/doi/10.1103/PhysRevLett.100.030402
[9] A. A. Sukhorukov, Z. Xu, and Y. S. Kivshar, "Nonlinear suppression of time reversals in $\mathcal{PT}$-symmetric optical couplers," *Phys. Rev. A*, vol. 82, Oct. 2010, Art. no. 043818. [Online]. Available: http://link.aps.org/doi/10.1103/PhysRevA.82.043818
[10] Y. Lumer, Y. Plotnik, M. C. Rechtsman, and M. Segev, "Nonlinearly induced $\mathcal{PT}$ transition in photonic systems," *Phys. Rev. Lett.*, vol. 111, Dec. 2013, Art. no. 263901. [Online]. Available: http://link.aps.org/doi/10.1103/PhysRevLett.111.263901
[11] H. Benisty, A. Lupu, and A. Degiron, "Transverse periodic $\mathcal{PT}$ symmetry for modal demultiplexing in optical waveguides," *Phys. Rev. A*, vol. 91, May 2015, Art. no. 053825. [Online]. Available: http://link.aps.org/doi/10.1103/PhysRevA.91.053825
[12] H. Hodaei, M.-A. Miri, M. Heinrich, D. N. Christodoulides, and M. Khajavikhan, "Parity-time–symmetric microring lasers," *Science*, vol. 346, no. 6212, pp. 975–978, 2014. [Online]. Available: http://www.sciencemag.org/content/346/6212/975.abstract
[13] W. Hayenga *et al.*, "Single mode broad area PT-symmetric microring lasers," presented at the Conf. Lasers Electro-Optics, San Jose, CA, USA, 2015, Paper FW1D.6.
[14] D. A. Antonosyan, A. S. Solntsev, and A. A. Sukhorukov, "Parity-time anti-symmetric parametric amplifier," presented at the Conf. Lasers Electro-Optics, San Jose, CA, USA, 2015, Paper JTu5A.16.
[15] L. Feng, Z. J. Wong, R.-M. Ma, Y. Wang, and X. Zhang, "Single-mode laser by parity-time symmetry breaking," *Science*, vol. 346, no. 6212, pp. 972–975, 2014. [Online]. Available: http://www.sciencemag.org/content/346/6212/972.abstract
[16] S. A. Maier, *Plasmonics: Fundamentals and Applications*. New York, NY, USA: Springer, 2007.
[17] W. L. Barnes, A. Dereux, and T. W. Ebbesen, "Surface plasmon subwavelength optics," *Nature*, vol. 424, pp. 824–830, Aug. 2003.
[18] S. I. Bozhevolnyi, V. S. Volkov, E. Devaux, J. Y. Laluet, and T. W. Ebbesen, "Channel plasmon subwavelength waveguide components including interferometers and ring resonators," *Nature*, vol. 440, pp. 508–511, Mar. 2006.
[19] H. Benisty, "Implementation of pt symmetric devices using plasmonics: Principle and applications," *Opt. Express*, vol. 19, no. 19, pp. 18004–18019, Sep. 2011. [Online]. Available: http://www.opticsexpress.org/abstract.cfm?URI=oe-19-19-18004
[20] H. Alaeian and J. A. Dionne, "Non-Hermitian nanophotonic and plasmonic waveguides," *Phys. Rev. B*, vol. 89, Feb. 2014, Art. no. 075136. [Online]. Available: http://link.aps.org/doi/10.1103/PhysRevB.89.075136
[21] H. Alaeian and J. A. Dionne, "Parity-time-symmetric plasmonic metamaterials," *Phys. Rev. A*, vol. 89, Mar. 2014, Art. no. 033829. [Online]. Available: http://link.aps.org/doi/10.1103/PhysRevA.89.033829
[22] T. Yang and K. B. Crozier, "Analysis of surface plasmon waves in metal-dielectric-metal structures and the criterion for negative refractive index," *Opt. Express*, vol. 17, no. 2, pp. 1136–1143, Jan. 2009.
[23] A. R. Davoyan *et al.*, "Mode transformation in waveguiding plasmonic structures," *Photon. Nanostruct., Fundam. Appl.*, vol. 9, pp. 207–212, 2011.
[24] J. R. Salgueiro and Y. S. Kivshar, "Complex modes in plasmonic nonlinear slot waveguides," *J. Opt.*, vol. 16, no. 114007, pp. 1–10, 2014.
[25] J. R. Salgueiro and Y. Kivshar, "Nonlinear couplers with tapered plasmonic waveguides," *Opt. Express*, vol. 20, no. 9, pp. 9403–9408, Apr. 2012.
[26] J. J. Burke, G. I. Stegeman, and T. Tamir, "Surface-polariton-like waves guided by thin, lossy metal films," *Phys. Rev. B*, vol. 33, pp. 5186–5201, 1986.
[27] S. E. Kocabas, G. Veronis, D. A. B. Miller, and S. Fan, "Modal analysis and coupling in metal-insulator-metal waveguides," *Phys. Rev. B*, vol. 79, 2009, Art. no. 035120.
[28] M.-S. Kwon and S.-Y. Shin, "Simple and fast numerical analysis of multilayer waveguide modes," *Opt. Commun.*, vol. 233, pp. 119–126, 2004.
[29] J. R. Salgueiro and Y. S. Kivshar, "Complex modes of nonlinear plasmonic waveguides," in *Proc. Int. Workshop Nonlinear Photon.*, Sep. 2013, pp. 14–16.
[30] W. H. Press, S. A. Teukolsky, W. T. Vetterling, and B. P. Flannery, *Numerical Recipes in C*, 2nd ed. Cambridge, U.K.: Cambridge Univ. Press, 1992.
[31] M. A. Ordal *et al.*, "Optical properties of the metals Al, Co, Cu, Au, Fe, Pb, Ni, Pd, Pt, Ag, Ti, and W in the infrared and far infrared," *Appl. Opt.*, vol. 22, no. 7, pp. 1099–1119, Apr. 1983.
[32] P. B. Johnson and R. W. Christy, "Optical constants of the noble metals," *Phys. Rev. B*, vol. 6, pp. 4370–4379, 1972.
[33] M. Conforti, M. Guasoni, and C. De Angelis, "Subwavelength diffraction management," *Opt. Lett.*, vol. 33, no. 22, pp. 2662–2664, Nov. 2008.
[34] S. A. Cummer, "An analysis of new and existing FDTD methods for isotropic cold plasma and a method for improving their accuracy," *IEEE Trans. Antennas Propag.*, vol. 45, no. 3, pp. 392–400, Mar. 1997.

José R. Salgueiro received the B.S. degree in physics from University of Santiago de Compostela, Santiago de Compostela, Spain and the M.S. and Ph.D. degrees in physics from University of Santiago de Compostela, Santiago de Compostela, in 1994 and 2001, respectively.

He has been a Research Fellow at the Nonlinear Physics Center, The Australian National University from 2002 to 2005. From 2005 to 2010, he had a tenure track position of the Ramón y Cajal program at the University of Vigo, Spain, where he is currently an Associate Professor. He has authored about 40 articles mainly on integrated optics and nonlinear and quantum optics. His current interests include nonlinear optics, plasmonics, photonic crystals, and THz physics.

Yuri S. Kivshar received the Ph.D. degree from Ukraine, in 1984. After working at several research centers in the U.S. and Europe, he moved to Australia in 1993 where he established the Nonlinear Physics Center. His research interests include nonlinear photonics, optical solitons, metamaterials, and nanophotonics. He is a Fellow of the Australian Academy of Science, OSA, APS, and IOP. He has received many awards including the Pnevmatikos Prize in Nonlinear Science (Greece), Lyle Medal (Australia), State Prize in Science and Technology (Ukraine), and Harrie Massey Medal (U.K.).